Review

Wenlong Zeng, Xiuli Yue* and Zhifei Dai*

Ultrasound contrast agents from microbubbles to biogenic gas vesicles

https://doi.org/10.1515/mr-2022-0020
Received June 22, 2022; accepted September 11, 2022;
published online October 19, 2022

Abstract: Microbubbles have been the earliest and most widely used ultrasound contrast agents by virtue of their unique features: such as non-toxicity, intravenous injectability, ability to cross the pulmonary capillary bed, and significant enhancement of echo signals for the duration of the examination, resulting in essential preclinical and clinical applications. The use of microbubbles functionalized with targeting ligands to bind to specific targets in the bloodstream has further enabled ultrasound molecular imaging. Nevertheless, it is very challenging to utilize targeted microbubbles for molecular imaging of extravascular targets due to their size. A series of acoustic nanomaterials have been developed for breaking free from this constraint. Especially, biogenic gas vesicles, gas-filled protein nanostructures from microorganisms, were engineered as the first biomolecular ultrasound contrast agents, opening the door for more direct visualization of cellular and molecular function by ultrasound imaging. The ordered protein shell structure and unique gas filling mechanism of biogenic gas vesicles endow them with excellent stability and attractive acoustic responses. What's more, their genetic encodability enables them to act as acoustic reporter genes. This article reviews the upgrading progresses of ultrasound contrast agents from microbubbles to biogenic gas vesicles, and the opportunities and challenges for the commercial and clinical translation of the nascent field of biomolecular ultrasound.

***Corresponding authors: Xiuli Yue**, School of Environment, Harbin Institute of Technology, No. 92 Xidazhi Street, Nangang District, Harbin 150001, Heilongjiang Province, China,
E-mail: xiulidx@163.com; and **Zhifei Dai**, Department of Biomedical Engineering, College of Future Technology, Peking University, No. 5 Yiheyuan Road, Haidian District, Beijing 100871, China,
E-mail: zhifei.dai@pku.edu.cn. https://orcid.org/0000-0001-6231-3692 (Z. Dai)
Wenlong Zeng, Department of Biomedical Engineering, College of Future Technology, Peking University, Beijing, China

Keywords: acoustic nanomaterials; acoustic reporter genes; biogenic gas vesicles; microbubbles; ultrasound contrast agents; ultrasound molecular imaging.

Introduction

Medical ultrasound imaging whose basic principle is receiving echo signals from tissue interfaces to form images has become one of the most popular diagnostic tools for clinical usage including obstetrics, cardiology, and radiology, due to advantages such as good safety, real time, low cost and high portability [1–5]. Nevertheless, tissue motion artifacts and weak echo signals from blood make ultrasound difficult to image microvasculature [6]. Therefore, ultrasound contrast agents (UCAs) are developed to improve the quality of ultrasound images. Once added to blood, UCAs with obviously different acoustic impedances from blood will strongly scatter the detection ultrasound to increase local echo signals and improve the sharpness and contrast of ultrasound images [7, 8].

In the 1960s, Gramiak et al. accidentally observed that weeny bubbles generated during rapid saline injections enhanced delineation of aortic blood flow [9]. Based on this phenomenon, early microbubbles (MBs) such as Levovist and Albunex were designed as small molecular gas bubbles stabilized by shells to obtain certain enhancement effects, but their poor stability and short circulation time limited their applications [10, 11]. After improvement via gas cores with high molecular weight and low solubility to enhance lifetime, the second-generation MBs with diameter distribution from 1 to 10 μm became main commercial UCAs widely used in clinical ultrasound contrast of tissues including the heart and liver [12, 13]. Moreover, MBs modified with specific ligands that aim at targets in the bloodstream extend their applications to ultrasound molecular imaging [14, 15].

Despite splendid performance in clinical practice, micron dimensions set up a barrier for MBs to applications in extravascular imaging [16, 17]. To break this limitation, organic acoustic nanomaterials with similar

components and properties to MBs have been exploited as nanoscale UCAs [18, 19], but their acoustic performances were still insufficient for clinical diagnosis. At the same time, researchers found that certain inorganic nanomaterials exhibited amusing echogenic properties as well [20, 21]. Although stable structures and easily modified surfaces promise inorganic nanomaterials a fascinating prospect for ultrasound imaging, biocompatibility and biosafety restrict their clinical translation [22, 23].

The visualization of molecular and cellular processes happening in organisms has momentous implications for the diagnosis and treatment of numerous diseases [24]. Fluorescent proteins are the most common and advanced means of realizing this purpose [25]. However, imaging deep tissues in large animals and even humans is a challenge for fluorescent proteins due to limited penetrability of visible light [26]. Conversely, ultrasound imaging that combines strong penetration with excellent spatial and temporal resolution suffers from lacking biomolecular reporters. It remained difficult to solve this issue until wonderful use of biogenic gas vesicles (BGVs) in ultrasound imaging was discovered recently. BGVs are gas-filled protein nanostructures expressed for adjusting buoyancy in some photosynthetic microbes [27]. Their first attempt as UCAs in 2014 inaugurated a new pathway for biomolecular ultrasound [28]. After altering shell proteins, engineered BGVs enabled multimodal ultrasound imaging and targeted contrast, establishing a universal biomolecular platform for diversified acoustic nanomaterials [29]. In addition, the creation of acoustic reporter genes (ARGs) suitable for microbes [30] and mammalian cells [31] made it possible for BGVs to replace fluorescent proteins. We aim to reveal infusive opportunities and challenges for the clinical translation of the biomolecular ultrasound via the evolution of UCAs from MBs to BGVs.

MBs used for efficient intravascular contrast

Compositions and evolution of MBs

MBs generally consist of an encapsulating shell and an inner gas core, both of which have significant impacts on the stability and acoustic performance [32, 33]. The shell can reduce release rate of gas cores to lengthen circulation time. Elastic shells enable MBs to resist higher levels of acoustic energy before rupture. The gas core is conducive to the overall stability and echogenicity through gas diffusion time reliant on molecular weight and solubility [34]. Furthermore, another notable parameter of MBs is their particle size that plays an important role in penetration, stability and echogenicity [35].

Proteins are the earliest and most biocompatible shell materials. Their clinical product (Optison) is approved for cardiac indications including left ventricular opacification and endocardial border definition [5]. However, poor stability together with immunogenicity confine applications and functionalization of MBs with protein shells [36, 37]. Inspired from biomembranes, phospholipids with good biocompatibility are designed as shells of MBs [38–40]. When there is an air-water interface, phospholipids will spontaneously assemble into a highly organized monolayer owing to the hydrophobic effect. Compared to protein shells, MBs with lipid shells exhibit preferable echogenicity and potential for molecular imaging because they are more pliable and easily modifiable [41]. Therefore, the other three MBs still in clinical use are all phospholipid shells, and their indications are extended to liver, breast and bladder lesions [5]. As another alternative shell material, polymers excel in hardness, compression resistance and stability. From the perspective of biosafety, MBs composed of biodegradable polymers such as poly (lactic-co-glycolic acid) (PLGA) and polyethylene glycol (PEG) are more clinically feasible [42, 43].

Gas cores of MBs have evolved from small molecular gases to bioinert gases with high molecular weight and low solubility, accompanied by enhanced stability of MBs because the latter require more time to escape from shells. Fluorinated gases including sulfur hexafluoride and perfluorocarbon (PFC) are main forces of clinical MBs at present [44].

Acoustics characteristics of MBs including the scattering cross section and resonant frequency are highly dependent on their particle sizes [45]. To balance echogenicity and penetration, MBs sizes are controlled in 1–10 μm where MBs can resonate with the ultrasound frequency range used in clinical diagnosis [46]. Nevertheless, dispersity mismatch between size distributions of commercial MBs and frequency bandwidths of clinical ultrasound scanners leads to incomplete excitation of MBs near resonant frequency [47]. Monodisperse MBs with uniform diameters are prepared via acoustic sorting and microfluidic production to solve this problem.

Imaging techniques based on acoustic responses of MBs

MBs mainly response to ultrasound in two forms. On the one hand, MBs strongly scatter incoming acoustic waves to generate bright spots on ultrasound images, due to their distinct acoustic impedance from surrounding fluids or tissues [48]. On the other hand, the high compressibility of gas cores and elasticity of shells allow MBs to oscillate nonlinearly in response to rapid variations of acoustic pressure, thereby producing harmonic signals different from the fundamental frequency [49].

Taking unique acoustic responses of MBs into consideration, two specific contrast modes have been developed to improve the signal-to-noise ratio and sensitivity of ultrasound imaging. The first technique separates mixed signals of MBs and tissues through high-pass or low-pass filtering to obtains a clear ultrasound image, on the basic of diverse scattering frequency ranges between MBs and tissues after transmission with a single ultrasound pulse [50]. The low susceptibility to tissue motion artifacts and permission to operate at high frame rates are main merits of this technique. The other technique utilizes nonlinear responses of MBs to continuous acoustic pulses with different characteristics, in contrast to linear responses from tissues [51]. Pulse inversion (PI) and amplitude modulation (AM) are the most commonly used schemes. PI consecutively emits two pulse sequences with the same frequency and amplitude but 180° phase reversal to increase MBs signals as well as counteract tissue signals by coherent summation [52]. AM realizes the same purpose using a series of pulses with different amplitudes [53]. What's more, contrast pulse sequence combining features of PI and AM has been reported as well [54]. The advent of these specific techniques further facilitates the prosperity of contrast-enhanced ultrasound.

Targeted MBs used for ultrasound molecular imaging

Molecular imaging able to monitor biological processes *in vivo* at the cell and molecular level is of great significance for early diagnosis and pathological analysis of diseases, but may be challengeable for ultrasound due to lack of suitable molecular probes. Not until targeted MBs appeared did this situation improve. Given that MBs are confined within vessels, targeted MBs consist of traditional MBs and ligands that direct at vascular endothelial markers [55, 56]. They have been widely used for imaging diseases such as tumor, inflammation together with thrombosis, and relevant clinical trials are ongoing [15].

Optimization of targeting biomechanics of MBs

In order to enable MBs to image target sites with initiative, celerity, high efficiency and stabilization, the choice of ligands is a crucial part. Above all, the basic condition of ligands is the ability to target vascular endothelial receptors including vascular endothelial growth factor receptor (VEGFR) and integrin $\alpha_v\beta_3$ [57]. Secondly, considering the demand of overcoming shear forces ascribed to blood flow, ligands with strong affinity are preferred so that MBs stay adherent. Another method to enhance adhesion efficiency is increasing the ligand density on MBs surfaces [37]. Finally, affected by the flow velocity of blood, the interaction between ligands and receptors must be a fast process, so small molecule ligands may be a superior choice [58].

Some studies indicated that modifying MBs with hydrophilic polymers such as PEG was favorable for their production and stability [59]. In addition, PEGylation can minimize nonspecific adhesions of MBs and uptake by reticuloendothelial system (RES) to decrease background signals and enhance targeting efficiency [60]. To prevent PEG chains from covering ligands, long PEG chains are usually used to connect ligands with MBs and provide adaptive space for the interaction between ligands and receptors, together with short and high-density PEG chains for stabilizing MBs [61].

Detection and signal enhancement of specifically adherent MBs

Echo signals from targeted MBs with specific adhesions are what we care for in ultrasound molecular imaging, and they need to be separate from other interference signals through some imaging strategies. Firstly, strategies based on nonlinear responses have been mentioned above for signal separation of MBs and background tissues. Then, the easiest way to differentiate signals of adherent and freely circulating MBs is leaving a sufficient waiting period after injection for clearing the latter, but it takes a long time and places high demands on the stability of MBs [37, 62]. A more common method utilizes high-intensity pulses to break all MBs in the region of interest (ROI) so that signals of adherent MBs are gained by deducting the post-rupture intensity from the pre-rupture intensity. Lack of real-time capability and potential biological effects are main defects of this method. An

alternative approach segregates signals of adherent MBs based on interframe characteristics of MBs including 'dwell time' threshold [37]. Lastly, false positives caused by nonspecific adhesions are ruled out via subtracting control signals of pure MBs without any ornament.

Targeted MBs for preclinical ultrasound molecular imaging

Targeted MBs can be applied in ultrasound molecular imaging of multiple diseases with the help of overexpressed vascular endothelial receptors. During angiogenesis that plays a vital role in tumor growth and metastasis, expressions of VEGFR, $\alpha_v\beta_3$ and endoglin are markedly upregulated. Therefore, targeted MBs aiming at these receptors or their combinations have been used to image cancer models including breast and pancreas in mice and rats [63–65]. These research results suggested that targeted MBs could accumulate at tumor sites and effectively enhance ultrasound signals of tumor angiogenesis. Thromboembolism possibly induced by high expressions of platelet glycoprotein IIb-IIIa is a primary cause why many cardiovascular diseases outbreak. Based on this receptor, targeted MBs were developed to improve the detection rate of thrombosis in rat and mouse models [66–68]. Farther studies using other receptors such as fibrin and tissue factor were reported as well [69]. Inflammation is a widespread process in injured or infected organisms, accompanied by specifically expressed markers including intercellular adhesion molecule-I, vascular endothelial cell adhesion molecule-I and E-/P-selectin. These markers and their combinations enabled targeted MBs to diagnose inflammation-related diseases such as atherosclerosis, myocardial ischemia, enteritis and immune rejection in many animal models [70–72].

Targeted MBs in clinical trials

BR55 comprised of a phospholipid shell encapsulating a mixed gas core of perfluorobutane and nitrogen is the first targeted MB in clinical trials. Modification with heterodimeric peptides that direct at VEGFR2 endows BR55 with unique potential in cancer diagnosis and therapy. After abundant preclinical assessments involving effectiveness and safety in various animal models, BR55 was approved for clinical research in human cancers. Smeenge et al. explored the feasibility and safety of BR55 for imaging human prostate tumor for the first time [14]. Their results indicated BR55 enhanced ultrasound contrast in 30 min without significant side effects and that the detection rate of malignant lesions reached 68%. Similar and even superior data were observed in clinical trials of breast and ovarian cancers [15]. These clinical results all declare that BR55 promises to be an important tool for noninvasive cancer screening.

Acoustic nanomaterials extend ultrasound to extravascular targets

Although targeted MBs have entered clinical trials, the size of MBs hinders their molecular imaging of extravascular targets. Therefore, acoustic nanomaterials with sufficient vascular penetration and easy modification were designed to improve the potential of ultrasound molecular imaging.

Nanobubbles

Nanobubbles (NBs) with nanometer diameters can be regarded as miniature versions of MBs, and their shells along with gas cores are homologous [73]. After adding appropriate surfactants during the preparation process to improve echogenicity and stability, NBs are able to achieve effective ultrasound contrast [74]. Wu et al. demonstrated that NBs synthesized with a pluronic surfactant possessed not only echo performance comparable to or better than Definity, but also better stability and longer circulation time [75]. Aggregation in tumor tissues due to the enhanced permeability and retention (EPR) effect endows NBs with a natural advantage in cancer diagnosis. Imaging results in tumor-bearing mouse models suggested that NBs visibly enhanced ultrasound contrast and lasted longer than MBs at tumor sites, corresponding to a larger accumulation of NBs observed in tumor cell spaces by fluorescent labeling and frozen slices [76]. Modification with ligands that target tumor markers can further increase the targeting efficiency of NBs to tumors. It was reported that ligand-modified NBs universally displayed a better contrast-enhanced effect or longer imaging time than unmodified MBs in multiple tumor models [77–80].

Phase-change nanodroplets

Phase-change nanodroplets (PCNDs) refer to nanodroplets (NDs) that can undergo phase transition upon exposure to energy radiations. They are composed of PFC droplets encapsulated with protein, lipid or polymer shells, and

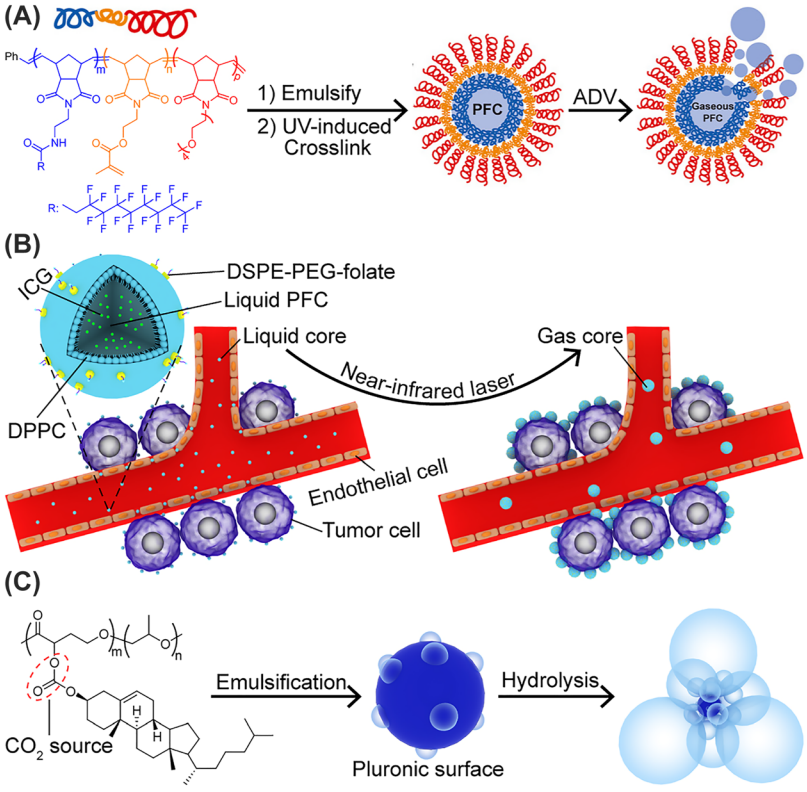

Figure 1: Organic acoustic nanomaterials used for ultrasound imaging. (A) PCNDs based on acoustic droplet vaporization. (B) Light-activated PCNDs. (C) Organic gas-generating nanoparticles based on carbonate copolymer. Reproduced with permission from [87, 89, 95], respectively. ADV, acoustic droplet vaporization; ICG, indocyanine green; OGGNPs, organic gas-generating nanoparticles; PCNDs, phase-change nanodroplets; PFC, perfluorocarbon; PEG, polyethylene glycol.

are superheated at physiological temperatures to stay metastable [81]. PCNDs can maintain their initial shapes and diameters for several hours after injection in the blood, which promises them enough time to penetrate and gather at the ROI [82, 83]. Once activated by energies, PCNDs will experience a transition from droplets to MBs where their acoustic impedances change markedly to effectively enhance echo signals. This ingenious "small to big" strategy is necessary for ultrasound imaging of PCNDs and endows them with potential in multiple targeting. At first, nanoscale sizes prior to activation enable PCNDs to aim at tumor sites through the EPR effect. Next, ligand modifications are able to further increase the targeting ability of PCNDs. In the end, energy activation in the ROI is also a type of spatial targeting, accompanied by reduced background signals. These advantages make PCNDs competitive in ultrasound molecular imaging.

Acoustic droplet vaporization

As the name implies, acoustic droplet vaporization (ADV) is a phenomenon that NDs are converted into MBs by thermal effects attributed to ultrasound, and it's the most convenient and common activation method of PCNDs. Li et al. encapsulated perfluorooctyl bromide NDs via a shell coupling folic acid and PEG to avoid clearance by RES and facilitate their targeting to tumors that overexpress folate receptors [84]. After activation by ultrasound *in vivo*, these targeted NDs showed a higher echo enhancement and longer contrast time at tumors with upregulated expression of folate receptor, in contrast to non-expressing tumors or non-targeted NDs. Similar results were reported by Liu and his co-workers, suggesting the possibility that targeted NDs displace targeted MBs as molecular UCAs [85]. However, comparison of imaging capabilities between targeted NDs and targeted MBs indicated that MBs provided better contrast than NDs despite quicker clearance from circulation [86]. This result means that targeted NDs may replace targeted MBs in extravascular rather than intravascular molecular imaging. To improve safety and acoustic sensitivity, NDs with low-boiling point PFCs were designed, and they could transform from liquid to gas via clinical ultrasound systems with better stability and less evaporation ahead of schedule (Figure 1A) [87].

Droplet vaporization by other energy radiations

To avoid the interference of ultrasound activation pulses on subsequent imaging pulses, other energy radiations independent of the ultrasound imaging process were

attempted. Numerous fluorescent dyes and photosensitizers make photoexcitation a good choice. Paproski et al. incorporated porphyrin into a lipid shell encapsulating liquid PFC to construct PCNDs, and attested their conversion into MBs induced by laser *in vitro* together with aggregation in tumors of chicken embryo models [88]. Farther *in vivo* ultrasound imaging of light-activated NDs was realized through a lipid shell co-loaded with liquid PFC and indocyanine green (ICG). Conjugation to folic acid enabled these NDs to exhibit greater accumulation and stronger ultrasound signals at tumor sites in mice (Figure 1B) [89]. PCNDs integrated with other optical absorbing materials and ligands were reported with similar good results [90, 91].

In view of limited penetration of light, other means were investigated to motivate PCNDs. Zhang et al. synthesized radiofrequency (RF)-responsive nanoparticles (NPs) with solid menthol encapsulated by PLGA [92]. After exposure to RF, menthol underwent continuous solid–liquid–gas triphase transformation to enhance ultrasound signals markedly. NDs activated by microwave or proton radiation were also reported for monitoring microwave ablation in tumor-bearing mice or verifying proton range during proton therapy, respectively [93, 94].

Organic gas-generating nanoparticles

Organic gas-generating nanoparticles (OGGNPs) are organic NPs that contain reactive or catalytic moieties to generate gases for ultrasound imaging when they reach the ROI. Min et al. designed carbonate copolymer-based NPs to release CO_2 bubbles through *in-situ* hydrolysis (Figure 1C) [95]. Their *in vivo* experiments displayed that these NPs accumulated at tumor sites of mice and produced ultrasound contrast for several hours. Another CO_2 generation mechanism based on chemical reaction with H_2O_2 was utilized to construct OGGNPs as well. These H_2O_2-responsive NPs were able to image many inflammatory diseases related to H_2O_2 overproduction such as hepatic injury and cancer, with obvious and continuous ultrasound signal enhancement [96–98]. Besides OGGNPs containing reactive moieties, catalytic OGGNPs were developed as well. Liu and his co-workers [99] immobilized catalase with dendritic mesoporous organosilica NPs to synthesize nanoreactors that exhibited catalytic activity for H_2O_2. After aggregation in tumors via the EPR effect, these NPs allowed ultrasound guidance for high intensity focused ultrasound (HIFU) ablation.

Inorganic nanoparticles

Alike to organic acoustic nanomaterials, inorganic inorganic nanoparticles (NPs) as UCAs can be roughly divided into three categories including NPs with natural echogenic properties, with energy conversion capabilities for phase change, and with reactive or catalytic moieties for gas generating. In spite of extensive research, their clinical application is unpromising due to poor biocompatibility and biosafety.

Silica NPs and carbon nanotubes are common inorganic materials with natural echogenic properties [100–102]. Casciaro et al. preliminarily studied acoustic behaviors of silica NPs, and demonstrated their availability for contrast-enhanced ultrasound at routine diagnostic frequencies [103]. After antibody modification to improve the targeting ability, silica NPs showed greater aggregation and more evident ultrasound signals in the ROI [104, 105]. Encapsulating PCFs or air in the hollow structure of silica NPs was conducive to the further improvement of their ultrasound imaging performance [106, 107]. Functionalized multi-walled carbon nanotubes were found to produce ultrasound signals comparable to Sonovue *in vitro* and possibly fit abdominal ultrasound [21]. They were developed as targeted UCAs for prostate cancer by conjugation to aptamers, and exhibited excellent targeting ability along with contrast effect both *in vitro* and *in vivo* ultrasound imaging [108].

Based on good energy conversion performances, some inorganic NPs including Au, iron oxide and Prussian blue are used to motivate liquid PFCs for ultrasound imaging. Li et al. prepared light-responsive nano UCAs by encapsulating hollow gold nanospheres and PFCs in liposomes [109]. Upon exposure to laser irradiation, photothermal effect of Au triggered phase change of PFCs to significantly enhance ultrasound signals of tumors. Similar gold-based NPs replaced liquid PFCs with solid menthol for extending imaging time to 30 min much longer than SonoVue [110]. As another photoabsorber, iron oxide was co-loaded with PFCs to design phase-change NPs for contrast-enhanced ultrasound of tumors in mice [111]. Nevertheless, magnetic energy converter is a more common usage of iron oxide. Magnetism-induced UCAs were constructed by combining iron oxide mesoporous NPs with PFCs, and dramatically increase ultrasound signals of both B mode and harmonic mode after magnetocaloric activation [112]. Other phase-change ultrasound contrast agents (UCAs) based on Prussian blue were proposed for ultrasound-guided tumor photothermal or HIFU therapy as well [113, 114].

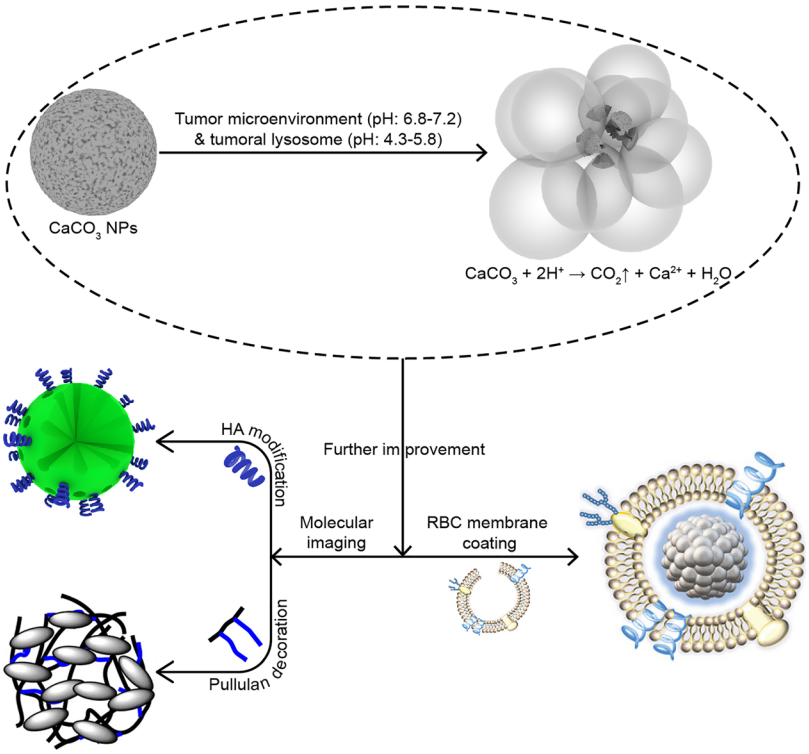

Figure 2: $CaCO_3$ inorganic nanoparticles as ultrasound contrast agents. Reproduced with permission from [117–119], respectively. HA, hyaluronic acid; NPs, nanoparticles; RBC, red blood cell; UCAs, ultrasound contrast agents.

MnO_2, Prussian blue and $CaCO_3$ are typical inorganic gas-generating NPs. Gao et al. encapsulated MnO_2 with hyaluronic acid (HA) to develop tumor-targeted nano UCAs that catalyzed excess H_2O_2 of tumor sites to generate oxygen for ultrasound imaging and photodynamic therapy [115]. Prussian blue NPs possessing alike H_2O_2 catalytic activity were also reported to image hepatic injury of murine models [116]. Compared with the two less degradable materials above, $CaCO_3$ NPs with better biodegradability are favored (Figure 2). Mesoporous $CaCO_3$ NPs bedecked with HA could be decomposed by the acidic microenvironment of tumors and ultrasound to release CO_2 for ultrasound diagnosis of tumors [117]. Modification with hepatoma-targeting pullulan helped $CaCO_3$ NPs to produce sixfold signal enhancement at tumor sites in mice [118]. Red blood cell (RBC) membranes were attempted as biomimetic coating of $CaCO_3$ NPs to further improve biocompatibility and restrain protein corona formation [119].

Biogenic gas vesicles applied as acoustic reporter genes (ARGs)

Biogenic gas vesicles (BGVs) were found in some microbes as buoyancy regulators to allow vertical movement in water for optimally capturing light and nutrients [27]. Their formation involves a cluster of 8–14 genes that encode one or two structural proteins as well as assembly factors including chaperones and nucleators [120, 121]. The shape and size of BGVs are highly reliant on their genetic species. Generally, mature BGVs are spindle-shaped or cylindrical protein with 100 nm–2 μm in length and 45–200 nm in width (Figure 3A, B) [27].

Different from common nanoscale bubbles, BGVs display abnormal physical stability due to their composition and unique gas retention mechanism. BGVs mainly include an internal gas compartment together with a 2-nm-thick protein shell self-assembled from amphiphilic gas vesicle protein A (GvpA) (Figure 3B) [27, 120]. GvpA with a molecular weight of 7–8 kDa may fold into a β sheet structure (Figure 3C), and form 4.6 nm-wide periodic ribs vertical to the long axis of BGV shells [122]. Another structural protein, gas vesicle protein C (GvpC), adheres to outer surfaces of certain BGVs to enhance stability (Figure 3D) [27]. Unlike gas pre-loaded in MBs with an unstable form, uniform pores on BGV shells permit free exchange between internal gases and gases in the ambient medium to reach dynamic equilibrium and exclude the water phase. As a result, the internal gas pressure of BGVs will be maintained at atmospheric pressure same as the outside, leading to particular stability of BGVs. However, once applied pressures exceed an explicit threshold correlative with genetics, BGVs will collapse and release gas [123, 124].

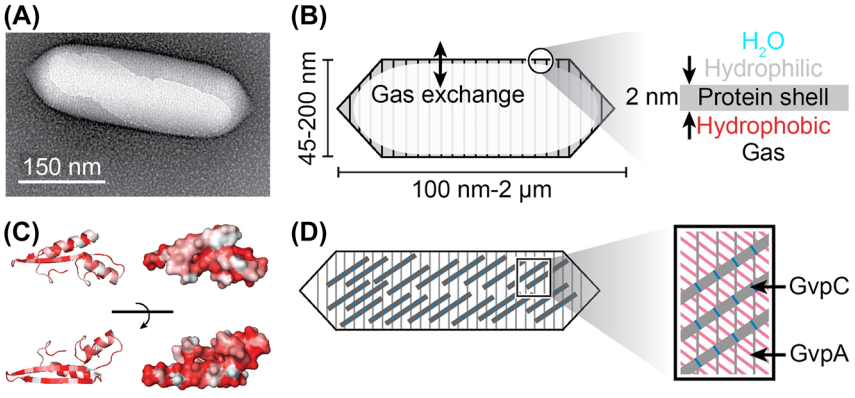

Figure 3: The shape, size, and composition of biogenic gas vesicles. (A) A TEM image of single Ana BGV. (B) A illustration of BGVs structure. (C) The beta folding of GvpA. (D) Protein arrays on the shell of BGVs. Reproduced with permission from [120]. BGVs, biogenic gas vesicles; GvpA, gas vesicle protein A; GvpC, gas vesicle protein C.

BGVs as a new type of biomolecular UCAs

Marked differences in acoustic impedance between internal gas compartments of BGVs and surrounding mediums enable BGVs to strongly scatter acoustic waves for ultrasound imaging, which was first testified by Shapiro et al. in 2014 [28]. They preliminary investigated acoustic performances of BGVs from different genetic species (Anabaena flos-aquae [Ana] and Halobacterium NRC-1 [Halo]). Imaging results in phantoms exhibited that the two BGVs both produced distinct ultrasound signals lasting for 1 week at concentrations as low as pM. Once gas compartments were destroyed by hydrostatic pressure, BGVs no longer showed ultrasound contrast (Figure 4A). To further improve contrast, harmonic detections of BGVs were carried out. As shown in Figure 4B, Halo BGVs generated plentiful harmonic signals for 3–5 times contrast enhancement after filtering while Ana BGVs did not. Imaging capabilities of intact Ana cells and purified BGVs from the same number of cells were compared as well. The 12-fold signal enhancement in intact cells implied attractive potential of BGVs as intracellular molecular probes and reporter genes (Figure 4C). Considering different collapse thresholds of each BGV, a successive collapse strategy by gradually increasing pressure was put forward to differentiate two BGVs in the same sample. Images of independent BGV were obtained from the layer-by-layer subtraction of composite images (Figure 4D). Finally, Halo BGVs were observed to enhance ultrasound signals in mice (Figure 4E), with great safety and degradability. These results all attested the feasibility of BGVs as new biomolecular UCAs.

Acoustic characteristics and imaging strategies of BGVs

It is necessary to explore acoustic characteristics of BGVs in more detail prior to their widespread applications in ultrasound imaging. Cherin et al. studied acoustic collapse pressures and behaviors of Halo BGVs exposed to ultrasound with center frequencies from 12.5 to 27.5 MHz [125]. Stress tests in phantoms displayed that acoustic collapse pressures at all transmission frequencies were nine times higher than the hydrostatic collapse pressure. This conspicuous difference may be ascribed to different pressurization rates. Hydrostatic pressure provides an equilibrium period of 7 s for internal gases of BGVs to flow out, thus reducing their pressure resistance. While effects of acoustic pressure take place in tens of ns that is shorter than gas exchange equilibrium time of BGVs, so gases have no time to overflow and help resist pressure. Under excitation with acoustic pressure below the collapse threshold, BGVs produced numerous harmonic signals marking their nonlinear oscillations. To investigate their harmonic generation mechanism, a simulation model that involves buckling and finite element analysis were adopted. The good agreement between test results and simulation data hinted that buckling was possibly responsible for harmonic signals of BGVs. And finite element analysis also certified that acoustic buckling pressure was equivalent to the hydrostatic collapse threshold, and supported the hypothesis that pressurization rates affected collapse thresholds. Moreover, calculation results of above two simulations speculated that a single BGV had a scattering cross section comparable to a single RBC but much smaller than a single MB, so maybe the generation of detectable ultrasound signals required a synergy of multiple BGVs. These discoveries have important implications for developing specific imaging strategies of BGVs to optimize their contrast.

Based on a preliminary cognition about acoustic characteristics of BGVs, specific imaging strategies were developed to improve ultrasound contrast of BGVs. Multipulse imaging methods of MBs were adopted for BGVs due to their alike harmonic signals. Maresca et al. compared

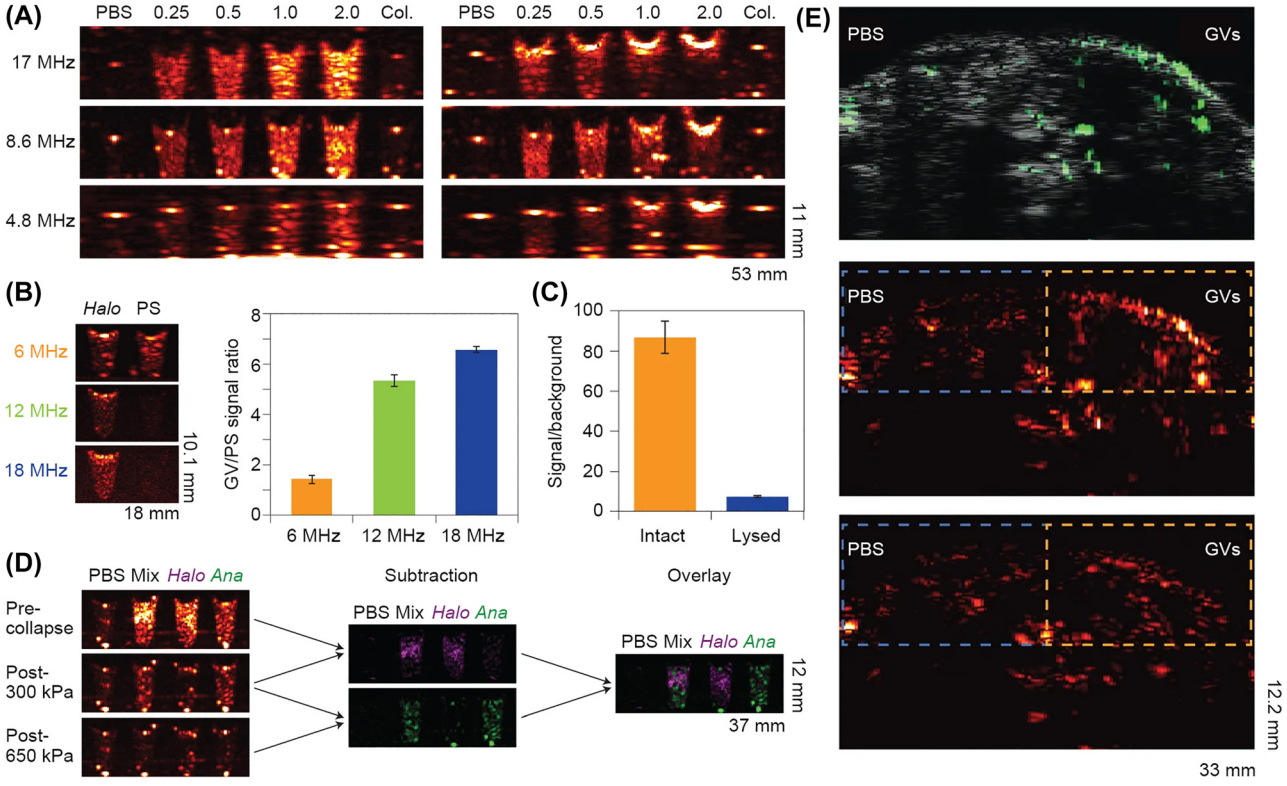

Figure 4: Ultrasound imaging of biogenic gas vesicles *in vitro* and *in vivo*. (A) Ultrasound images of phantoms containing Ana BGVs (left) and Halo BGVs (right) with different concentrations. (B) Harmonic images of Halo BGVs and polystyrene microspheres. (C) Ultrasound images (left) of Ana cells and Ana BGVs, along with integrated signal intensity (right) of left. (D) Multiplexed imaging with Halo and Ana BGVs. (E) Ultrasound images of mouse lower abdomen injected with Halo BGVs. Top: overlay of harmonic images (green) on gray images; middle and bottom: harmonic images before and after BGVs collapse. Reproduced with permission from [28]. BGVs, biogenic gas vesicles; PS, polystyrene.

adaptabilities of AM and PI to BGVs via simulations and phantoms [126]. Simulation calculation results revealed that AM generated signals at both fundamental and harmonic frequencies while PI only retained harmonic signals. During phantom tests, AM images showed almost exclusive harmonic signals of BGVs while PI images contained partial linear artifact. Hence, AM might be a more appropriate method for BGVs due to its higher harmonic contrast. Compared to B mode, AM mode easily identified cells containing BGVs and clearly imaged BGVs in mouse colons. These results all proved that AM was an effective strategy for BGVs-specific nonlinear imaging, contributing to promote the progress of BGVs as UCAs.

Although AM can effectively distinguish BGVs from linear scatterers such as tissues, acoustic waves passing through BGVs will also acquire nonlinearities, causing strong image artifacts in downstream tissues of BGVs. To address this issue, an imaging technique called cross-AM (xAM) was introduced on the basic of a guess that nonlinear interactions of counter-propagating acoustic waves were ineffective in biological tissues [127]. xAM synchronously transmitted two plane waves that propagate in an X-shape to minimize cumulate nonlinear interactions resulted from collinear wave diffusion. Simulation data analysis manifested that the nonlinearity owing to wave propagation was inversely related to cross angles of the two plane waves in xAM, which was further confirmed in phantom tests. As the cross angle gradually increased above 16.5°, image artifacts at the far end of BGVs in phantoms gradually decreased to a negligible level. Imaging in gastrointestinal tracts of mice also verified the superior imaging performance of xAM. The ring-shaped BGVs inclusion was almost completely visible in the xAM image, with legible internal and external outlines as well as few artifacts nearby, while the AM image only exhibited partial inclusion accompanied by obvious artifacts. Besides BGVs, xAM promises to be applied in MBs to improve the accuracy of clinical ultrasound diagnosis.

Molecular and functional ultrasound imaging based on BGVs

Despite targeting tumors via the EPR effect, ultrasound contrast of BGVs at tumor sites are less-than-ideal on account of their rapid uptake into RES. Some means of circumventing RES engulfment were tried to improve this situation [128]. Without any treatment of BGVs or RES, ultrasound signals of BGVs only lasted for a short time in tumors, and tumor reperfusion signals after blasting *in situ* were not evident as well, implying quick clearance of BGVs in the blood. If phagocytosis of RES was saturated by an initial injection of BGVs, the following second injection would prolong imaging time and enhance signal intensity of reperfusion at tumor sites, but the high dose of this method may cause excess cost and safety problems. A similar approach blocking the phagocytic activity of RES through reagents such as Intralipid and $GdCl_3$ achieved same effects, whereas it damaged normal functions of organisms meanwhile. The safer and more effective way was to shield BGVs by PEGylation. Four PEG chains with different molecular weight were respectively conjugated to BGVs for researching influences of PEG chain length. As expected, PEG chains with molecular weights of 2, 5, and 10 kDa successfully protected BGVs and prolonged contrast time in tumors. Confusingly, 5 and 10 kDa PEG chains also enhanced reperfusion signals of BGVs while 2 kDa PEG chain did not. BGVs modified with 15 kDa PEG chain didn't perform better than natural BGVs without PEGylation, perhaps because steric hindrance between macromolecular chains decreased the amount of PEG attached to BGVs surfaces. Hence, PEGylation with 5 and 10 kDa PEG chains is a feasible method of transforming BGVs into molecular UCAs.

BGVs were designed as superior targeted UCAs through PEGylation with 5 kDa PEG chains for prolonged circulation time and embellishment with HA for actively targeting tumors [129]. *In vitro* experiments demonstrated that these modifications conduced to tumor targeting and immune escape of BGVs, without injuring their stability and acoustic responses. *In vivo* metabolisms of these bi-modified BGVs (BMBGVs) and control groups also supported this verdict. Real-time fluorescence imaging showed that ICG-labeled BMBGVs mainly concentrated at tumor sites 6 h after injection and maintained strong fluorescent signals for more than 48 h while natural BGVs or BGVs only modified with HA mostly located in RES and was quickly excreted in tumors. Subsequent ultrasound imaging also showed infusive results: BMBGVs produced much stronger and more lasting ultrasound signals than natural BGVs and HA-modified BGVs at tumor sites. These results jointly announces the birth of new nanoscale molecular UCAs that are expected to replace targeted MBs (BR55) in clinical trials.

BGVs can also be used for functional ultrasound (fUS), an imaging method that reflects local changes of cerebral blood volume owing to neural activity through ultrafast frame rates [130]. FUS is widely applied in research of basic neuroscience including imaging brain functions with a resolution of 100 μm [131, 132]. However, the acoustic attenuation and distortion resulted from skulls ask for craniotomy imaging that destroys the noninvasive nature of fUS. An alternative method for compensation is injecting MBs into the blood, but it suffers from rapid signal loss, high dose along with extra random fluctuations [133]. BGVs may be able to overcome these limitations because of their physical stability, monodispersity and nanoscale size. Maresca et al. compared effects of Ana BGVs and commercial MBs on enhancing hemodynamic fUS [134]. Phantom tests indicated that BGVs could withstand higher acoustic pressure and accurately report lower flow rates as opposed to MBs, corresponding to higher dynamic range and better resolution. *In vivo* evaluation manifested that BGVs enhanced Doppler and fUS signals with much less fluctuation than MBs, which enabled BGVs to realize more effective signal amplification. After modification to increase circulation time and contrast, BGVs may become the first choice of fUS contrast agents.

Molecular engineering of BGVs provides a universal biomolecular platform

GvpC, a structural protein for enhancing stability, can be replaced, modified or removed without destroying vesicle structures of BGVs, which provides a natural molecular platform for constructing BGVs with various properties. Impacts of changing GvpC on Ana BGVs were explored by Lakshmanan and his colleagues [29]. They first removed natural GvpC on shells of Ana BGVs with urea to retain complete GvpA skeletons. Ana BGVs with bereft GvpC were then incubated with excess GvpC variants recombinantly expressed in *Escherichia coli* to deposit a new GvpC layer (Figure 5A). A series of homologous Ana BGVs with different characters was prepared for follow-up research by changing types of GvpC variants.

Distinct differences of acoustic collapse thresholds between Ana BGVs with GvpC and Halo BGVs without GvpC hinted that GvpC might affect mechanical properties of BGVs [28]. This hypothesis was further confirmed using homologous Ana BGVs to exclude the GvpA variable [29]. Three types of engineered Ana BGVs without

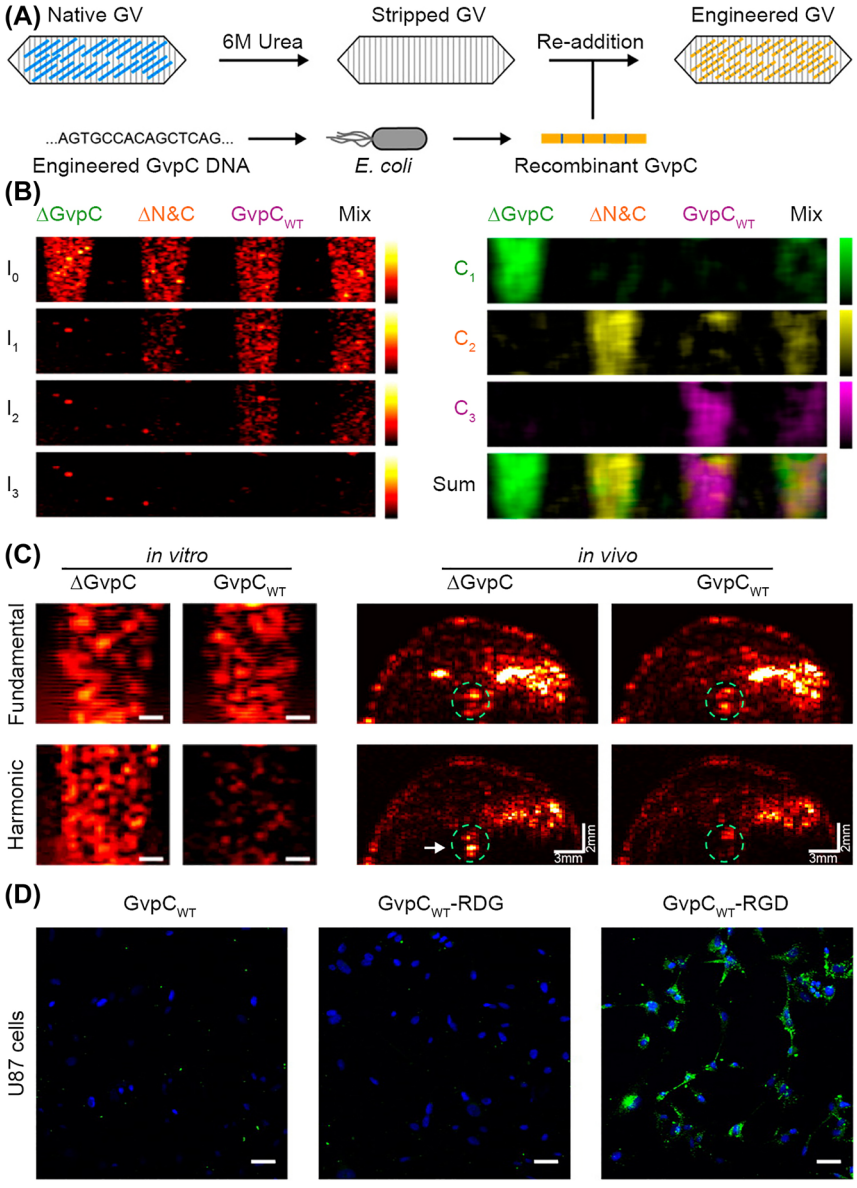

Figure 5: Regulating acoustic responses and targeting capabilities of biogenic gas vesicles through engineered gas vesicle protein C. (A) Paradigm for modular engineering of Ana BGVs. (B) Multiplexed imaging of Ana BGVs with different engineered GvpC. Left: mixed images; right: unmixed images processed from raw data in left. (C) Harmonic imaging of ΔGvpC and $GvpC_{WT}$ *in vitro* and *in vivo*. (D) Confocal fluorescence images of $GvpC_{WT}$ (green) modified with RDG and RGD after 24 h incubation with U87 glioblastoma cells (blue). Reproduced with permission from [29]. BGVs, biogenic gas vesicles; GvpC, gas vesicle protein C; GvpCWT, GvpC alike to wild type; ΔGvpC, Ana BGVs without GvpC.

GvpC (ΔGvpC), with truncated GvpC (ΔN&C) and with GvpC alike to wild type ($GvpC_{WT}$) showed hydrostatic and acoustic collapse pressures from low to high, respectively. Therefore, their mixture could perform multiplexed imaging by gradually increasing intensities of acoustic pulses. To analyze complex multiplexed images, a strategy that extracted and calculated signal differences between images under different pressures by matrix was introduced for splitting pressure spectral and forming unmixed images of each BGV (Figure 5B). This multiplexed imaging and its analytical strategy can easily expand to combinations of more different BGVs, facilitating simultaneous ultrasound imaging of multiple targets in a same sample.

Besides collapse thresholds, GvpC may impact harmonic signals related to shell mechanics of Ana BGVs. *In vitro* experiments showed that ΔGvpC produced a harmonic signal peak while $GvpC_{WT}$ only responded linearly, under a same transmission frequency. After bandpass filtering, the corresponding harmonic signal intensity of ΔGvpC was 3–4 times higher than $GvpC_{WT}$ with comparable fundamental frequency signals. Similar phenomena were observed in ultrasound imaging *in vivo* (Figure 5C) [29]. These results manifest that regulating GvpC can create BGVs with diversified harmonic responses to meet different imaging needs.

Integrations of GvpC with other peptides help control behaviors and distributions of BGVs *in vivo*. For instance,

fusing GvpC with charged proteins altered surface charges to affect aggregation and adsorption of BGVs in the blood. Fusion of GvpC and specific ligands targeting tumors promoted capture of BGVs by tumor cells (Figure 5D). Fusing of GvpC with sequences recognized and acted on by specific proteases achieve protease-responsive nonlinear ultrasound contrast [135]. To simplify and standardize the fusion process, GvpC was pre-fused with SpyTag to quickly bond other proteins fused with SpyCatcher, increasing the efficiency of BGVs functionalization markedly [29].

In a word, molecular engineering potentials closely associated with GvpC enable BGVs to acquire greater ultrasonic performances and a wider range of applications through simple modification, which provides a universal biomolecular platform for ultrasound molecular imaging.

BGVs applied as acoustic reporter genes

In view of poor penetration of optical reporter genes (ORGs), acoustic reporter genes (ARGs) based on BGVs are developed for imaging cells deep in organisms. Multigene clusters encoding BGVs were first heterologously expressed in certain bacteria owing to homologous heredity of prokaryotes. As reported by Farhadi and his coworkers, the BGVs gene cluster from *Bacillus megaterium* was transfected into *E. coli* and produced small Mega BGVs whose weak echogenicity was insufficient for cells to be detected by ultrasound [136]. Conversely, the gene cluster encoding highly echogenic Ana BGVs couldn't be expressed in *E. coli*. To mediate this contradiction, Bourdeau et al. integrated structural GvpA and GvpC genes from Anabaena flos-aquae with accessory genes from *B. megaterium* to construct a gene cluster expressing highly echogenic BGVs in *E. coli* [30]. This engineered gene cluster called ARG1 expressed large BGVs occupying about 10% of intracellular volume, to form *E. coli* detectable by ultrasound at a low detection limit enough for general *in vivo* imaging. Inspired by engineered GvpC at a protein level, ARGs containing different GvpC genes allowed multiplexed ultrasound imaging as well (Figure 6A), similar to fluorescent proteins with different spectra. Based on preliminary *in vitro* experiments, *in vivo* evaluations were performed and showed that ARGs located *E. coli* in mouse colons more accurately than ORGs (Figure 6B and Figure 6C). Besides *E. coli*, ARGs could be generalized to other strains for cell imaging in tumors together with high-throughput screening of colony according to acoustic phenotypes (Figure 6D). These results all demonstrate that ARGs able to visualize microbes in organisms may play an important role in exploring microbial processes relevant to occurrence, development or treatment of diseases.

Mammalian cells rather than microbes are preferred expression media for ARGs because they can directly reflect generation mechanism and development process of diseases in human bodies. Nevertheless, genetic differences between eukaryotes and prokaryotes pose challenges to developing ARGs for mammalian cells [137, 138]. To solve this issue, three BGVs gene clusters from different sources were transfected into human embryonic kidney (HEK) 293 cells through optimized codons for human expression, to screen effective genes for BGVs generation. As a result, only nine BGVs genes from *B. megaterium* produced BGVs in HEK293 cells. Then, three plasmids containing different subsets of these nine genes were constructed to achieve stable and consistent expression of BGVs, and they were called mammalian ARGs (mARGs). After transfecting mARG into HEK293 cells, the cell line yielding the most BGVs was named mARG-HEK, and it averagely produced 45 BGVs with mean widths of 64 nm and mean lengths of 274 nm per cell. Ultrasound imaging of mARG-HEK cells compared signal differences before and after BGVs collapse caused by AM pulses to eliminate background signals (Figure 6E). *In vitro* experiments indicated that mARG-HEK cells were easily distinguished from control cells even when the former only accounted for a small proportion of the two cells mixture (Figure 6F). Interestingly, this collapse-based imaging was reproducible due to re-expressions of BGVs. Similar phenomena were observed in ultrasound imaging of mouse tumors. The periphery of tumors inoculated with mARG-HEK cells exhibited obvious ultrasound contrast (Figure 6G), corresponding to BGVs expressions caused by tumor neovascularization, which was more accurate than fluorescence imaging. Four days later, renascent ultrasound signals at tumor sites testified re-expressions of BGVs [31].

Although ARGs capable of producing obvious and renewable ultrasound contrast in mammalian cells have been developed, the sensitivity of visualizing ARG-expressing cells is still insufficient. Hence, an ultrasensitive ARG imaging paradigm, burst ultrasound reconstructed with signal templates (BURST) was proposed. BURST separated the temporal dynamics of the strong, transient signals produced during GV collapse from background scattering. It increased cellular imaging sensitivity by more than 1,000 times to achieve quantitative single-cell imaging [139].

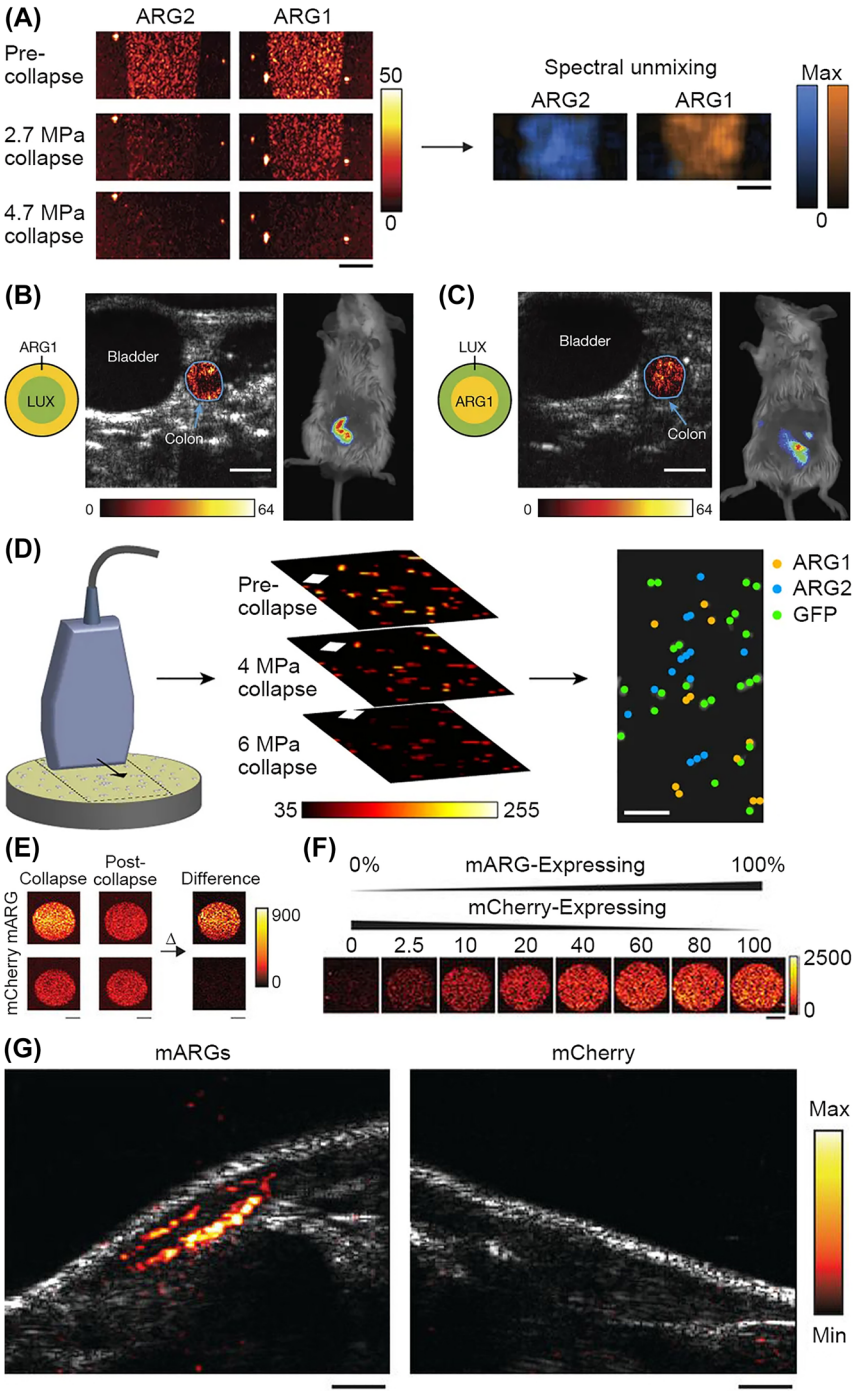

Figure 6: Biogenic gas vesicles as acoustic reporter genes in microbes (A–D) and mammalian cells (E–G). (A) Multiplexed imaging of bacteria containing ARGs with different collapse thresholds (arg1 and arg2) in phantoms. (B) and (C) Images of ARG1 and a ORG (LUX) in gastrointestinal tracts with different bacteria arrays. Left: ultrasound images; right: fluorescence images. (D) ARGs used for acoustic colony screening. Reproduced with permission from [30]. (E) Ultrasound images of mARG-HEK cells and control cells (mCherry-HEK) *in vitro*, before and after acoustic collapse. (F) Ultrasound images of mixtures with different mARG-HEK and mCherry-HEK cell ratios. (G) Ultrasound images of mARG-HEK and mCherry-HEK cells in tumors. Reproduced with permission from [31]. ARGs, acoustic reporter genes; BGVs, biogenic gas vesicles; mARG-HEK, mammalian ARG-human embryonic kidney; mCherry-HEK, mCherry-human embryonic kidney; ORG, optical reporter gene.

Conclusion and future challenges

Ultrasound imaging is one of the most popular imaging modes in clinical diagnosis at present, which is inseparable from splendid contrast effects of UCAs. As the earliest UCA, MB is also the exclusive UCA approved by FDA for clinical applications because of its excellent echogenicity, good stability, nonlinear response distinct from human tissues and recognized safety, making great contributions to clinical promotion of ultrasound imaging. Particularly, harmonic signals caused by MBs nonlinear oscillation can significantly increase contrast specificity through multipulse imaging strategies such as PI and AM. What's more, targeted MB (BR55) that aim at VEGFR2 is undergoing clinical trials and performs well in ultrasound molecular imaging of human prostate, ovary and breast

cancers, under the premise of abundant preclinical studies proving safety and effectiveness. It is believed that BR55 and even other targeted MBs will be used for clinical practice in the near future to expand the application scope, specificity and accuracy of ultrasound imaging.

To extend ultrasound from intravascular imaging to extravascular imaging, a series of organic and inorganic acoustic nanomaterials that can pass through blood vessel walls has been designed as substitutes of MBs. Most of them create strong ultrasound contrasts by phase-change or gas-generating strategies for MBs formation. They are widely used for tumor imaging with the assist of EPR effect-induced natural targeting, and present vast potential in ultrasound molecular imaging due to their convenient modification. Nevertheless, their biocompatibility and safety need to be verified in detail, so their clinical applications may still be far away.

As the first UCA derived from organisms, BGVs display attractive prospects for clinical transformation. Firstly, natural BGVs produce obvious ultrasound contrast at concentrations as low as pM, and farther improvement can be achieved by collapse-mediated signal differences and harmonic detection. After PEGylation and embellishment with specific ligands, BGVs are appropriate for ultrasound molecular imaging. Then, encodability and replaceability of GvpC provide a natural molecular platform for BGVs to regulate their collapse thresholds, harmonic signals, *in vivo* behaviors and distributions, so that multiplexed imaging, harmonic imaging and molecular imaging can come true. Lastly, as an alternative to ORGs, ARGs encoding BGVs have been heterologously expressed in microbes and mammalian cells, which is of significance to visualizing pathogenesis, development process and microbial effects of diseases deep in human bodies at the cellular level. However, the composition of ARGs needs to be simplified so that their expressions are more controllable and robust.

Looking back at the evolution from MBs to BGVs, UCAs tend to be miniaturized and biogenic, declaring the research hotspot for future clinical UCAs. As the first biomolecular UCAs in line with this evolutionary trend, BGVs exhibit excellent capabilities of contrast-enhanced ultrasound. However, the acoustic response mechanism of BGVs needs to be deeply investigated, and molecular engineering of BGVs as well as construction of ARGs require further validation and simplification. In addition, ensuing safety hazards and genetic differences between different species also pose challenges to clinical transformation of BGVs. Therefore, maybe nanoscale echo scatterers in animals and even humans will be a better choice, while it calls for a long process of exploration and verification. Finally, the transfer and improvement of clinical imaging methods from MBs to BGVs and the development of corresponding clinical imaging instruments are also major challenges.

Research funding: This work was financially supported by National Project for Research and Development of Major Scientific Instruments (No. 81727803), National Natural Science Foundation of China (No. 82071980), State Key Program of National Natural Science of China (No. 81930047) and Projects of International Cooperation and Exchanges NSFC-PSF (No. 31961143003).

Author contributions: Wenlong Zeng: Literature review and analysis, Writing original Draft. Xiuli Yue and Zhifei Dai: Conceptualization, Review & Editing, Funding acquisition. All authors have accepted responsibility for the entire content of this manuscript and approved its submission.

Competing interests: Authors state no conflict of interest.

Ethical approval: Not applicable.

References

1. Chen M, Liang XL, Dai ZF. Manganese(iii)-chelated porphyrin microbubbles for enhanced ultrasound/mr bimodal tumor imaging through ultrasound-mediated micro-to-nano conversion. Nanoscale 2019;11:10178–82.
2. Ke H, Wang J, Tong S, Jin Y, Wang S, Qu E, et al. Gold nanoshelled liquid perfluorocarbon magnetic nanocapsules: a nanotheranostic platform for bimodal ultrasound/magnetic resonance imaging guided photothermal tumor ablation. Theranostics 2013;4:12–23.
3. Jin Y, Wang J, Ke H, Wang S, Dai Z. Graphene oxide modified pla microcapsules containing gold nanoparticles for ultrasonic/CT bimodal imaging guided photothermal tumor therapy. Biomaterials 2013;34:4794–802.
4. Zha ZB, Wang JR, Qu EZ, Zhang SH, Jin YS, Wang SM, et al. Polypyrrole hollow microspheres as echogenic photothermal agent for ultrasound imaging guided tumor ablation. Sci Rep 2013;3:1–8.
5. Yusefi H, Helfield B. Ultrasound contrast imaging: fundamentals and emerging technology. Front Phys 2022;10:791145.
6. Pellow C, Goertz DE, Zheng G. Breaking free from vascular confinement: status and prospects for submicron ultrasound contrast agents. Wires Nanomed Nanobiotechnol 2018;10: e1502.
7. Ke H, Wang J, Dai Z, Jin Y, Qu E, Xing Z, et al. Gold-nanoshelled microcapsules: a theranostic agent for ultrasound contrast imaging and photothermal therapy. Angew Chem Int Ed Engl 2011;50:3017–21.
8. Ke HT, Wang JR, Dai ZF, Jin YS, Qu EZ, Xing ZW, et al. Bifunctional gold nanorod-loaded polymeric microcapsules for both

contrast-enhanced ultrasound imaging and photothermal therapy. J Mater Chem 2011;21:5561–4.
9. Gramiak R, Shah PM. Echocardiography of the aortic root. Invest Radiol 1968;3:356–66.
10. Zullino S, Argenziano M, Stura I, Guiot C, Cavalli R. From micro- to nano-multifunctional theranostic platform: effective ultrasound imaging is not just a matter of scale. Mol Imag 2018; 17:1536012118778216.
11. Ignee A, Atkinson NSS, Schuessler G, Dietrich CF. Ultrasound contrast agents. Endosc Ultrasound 2016;5:355–62.
12. McDonald DM, Choyke PL. Imaging of angiogenesis: from microscope to clinic. Nat Med 2003;9:713–25.
13. Mehta KS, Lee JJ, Taha AA, Avgerinos E, Chaer RA. Vascular applications of contrast-enhanced ultrasound imaging. J Vasc Surg 2017;66:266–74.
14. Smeenge M, Tranquart F, Mannaerts CK, de Reijke TM, van de Vijver MJ, Laguna MP, et al. First-in-human ultrasound molecular imaging with a VEGFR2-specific ultrasound molecular contrast agent (BR55) in prostate cancer a safety and feasibility pilot study. Invest Radiol 2017;52:419–27.
15. Willmann JK, Bonomo L, Testa AC, Rinaldi P, Rindi G, Valluru KS, et al. Ultrasound molecular imaging with BR55 in patients with breast and ovarian lesions: first-in-human results. J Clin Oncol 2017;35:2133–40.
16. Liang XL, Xu YX, Gao C, Zhou YM, Zhang NS, Dai ZF. Ultrasound contrast agent microbubbles with ultrahigh loading capacity of camptothecin and floxuridine for enhancing tumor accumulation and combined chemotherapeutic efficacy. NPG Asia Mater 2018;10:761–74.
17. You YJ, Liang XL, Yin TH, Chen M, Qiu C, Gao C, et al. Porphyrin-grafted lipid microbubbles for the enhanced efficacy of photodynamic therapy in prostate cancer through ultrasound-controlled in situ accumulation. Theranostics 2018;8:1665–77.
18. Guvener N, Appold L, de Lorenzi F, Golombek SK, Rizzo LY, Lammers T, et al. Recent advances in ultrasound-based diagnosis and therapy with micro- and nanometer-sized formulations. Methods 2017;130:4–13.
19. Liu RF, Tang J, Xu YX, Dai ZF. Bioluminescence imaging of inflammation in vivo based on bioluminescence and fluorescence resonance energy transfer using nanobubble ultrasound contrast agent. ACS Nano 2019;13:5124–32.
20. Milgroom A, Intrator M, Madhavan K, Mazzaro L, Shandas R, Liu BL, et al. Mesoporous silica nanoparticles as a breast-cancer targeting ultrasound contrast agent. Colloids Surf, B 2014;116:652–7.
21. Delogu LG, Vidili G, Venturelli E, Menard-Moyon C, Zoroddu MA, Pilo G, et al. Functionalized multiwalled carbon nanotubes as ultrasound contrast agents. Proc Natl Acad Sci USA 2012;109: 16612–7.
22. Yang K, Feng LZ, Shi XZ, Liu Z. Nano-graphene in biomedicine: theranostic applications. Chem Soc Rev 2013;42:530–47.
23. Chen Y, Chen HR, Shi JL. In vivo bio-safety evaluations and diagnostic/therapeutic applications of chemically designed mesoporous silica nanoparticles. Adv Mater 2013;25:3144–76.
24. Dean KM, Palmer AE. Advances in fluorescence labeling strategies for dynamic cellular imaging. Nat Chem Biol 2014;10: 512–23.
25. Chu J, Oh Y, Sens A, Ataie N, Dana H, Macklin JJ, et al. A bright cyan-excitable orange fluorescent protein facilitates dual-emission microscopy and enhances bioluminescence imaging in vivo. Nat Biotechnol 2016;34:760–7.
26. Ntziachristos V. Going deeper than microscopy: the optical imaging Frontier in biology. Nat Methods 2010;7:603–14.
27. Pfeifer F. Distribution, formation and regulation of gas vesicles. Nat Rev Microbiol 2012;10:705–15.
28. Shapiro MG, Goodwill PW, Neogy A, Yin M, Foster FS, Schaffer DV, et al. Biogenic gas nanostructures as ultrasonic molecular reporters. Nat Nanotechnol 2014;9:311–6.
29. Lakshmanan A, Farhadi A, Nety SP, Lee-Gosselin A, Bourdeau RW, Maresca D, et al. Molecular engineering of acoustic protein nanostructures. ACS Nano 2016;10: 7314–22.
30. Bourdeau RW, Lee-Gosselin A, Lakshmanan A, Farhadi A, Kumar SR, Nety SP, et al. Acoustic reporter genes for noninvasive imaging of microorganisms in mammalian hosts. Nature 2018;553:86–90.
31. Farhadi A, Ho GH, Sawyer DP, Bourdeau RW, Shapiro MG. Ultrasound imaging of gene expression in mammalian cells. Science 2019;365:1469–75.
32. Newsome IG, Kierski TM, Dayton PA. Assessment of the superharmonic response of microbubble contrast agents for acoustic angiography as a function of microbubble parameters. Ultrasound Med Biol 2019;45:2515–24.
33. Hameed S, Zhang MM, Bhattarai P, Mustafa G, Dai ZF. Enhancing cancer therapeutic efficacy through ultrasound-mediated micro-to-nano conversion. Wires Nanomed Nanobiotechnol 2020;12: e1604.
34. Rafailidis V, Huang DY, Yusuf GT, Sidhu PS. General principles and overview of vascular contrast-enhanced ultrasonography. Ultrasonography 2020;39:22–42.
35. Gnyawali V, Moon BU, Kieda J, Karshafian R, Kolios MC, Tsai SSH. Honey, I shrunk the bubbles: microfluidic vacuum shrinkage of lipid-stabilized microbubbles. Soft Matter 2017;13: 4011–6.
36. Rovers TAM, Sala G, van der Linden E, Meinders MBJ. Effect of temperature and pressure on the stability of protein microbubbles. ACS Appl Mater Interfaces 2016;8:333–40.
37. Wang SY, Hossack JA, Klibanov AL. Targeting of microbubbles: contrast agents for ultrasound molecular imaging. J Drug Target 2018;26:420–34.
38. Lin X, Zhang X, Wang S, Liang X, Xu Y, Chen M, et al. Intraoperative identification and guidance of breast cancer microfoci using ultrasound and near-infrared fluorescence dual-modality imaging. ACS Appl Bio Mater 2019;2:2252–61.
39. Chen M, Liang XL, Gao C, Zhao RR, Zhang NS, Wang SM, et al. Ultrasound triggered conversion of porphyrin/camptothecin-fluoroxyuridine triad microbubbles into nanoparticles overcomes multidrug resistance in colorectal cancer. ACS Nano 2018;12:7312–26.
40. Xu YX, Liang XL, Bhattarai P, Sun Y, Zhou YM, Wang SM, et al. Enhancing therapeutic efficacy of combined cancer phototherapy by ultrasound-mediated in situ conversion of near-infrared cyanine/porphyrin microbubbles into nanoparticles. Adv Funct Mater 2017;27:1704096.
41. Luan Y, Faez T, Gelderblom E, Skachkov I, Geers B, Lentacker I, et al. Acoustical properties of individual liposome-loaded microbubbles. Ultrasound Med Biol 2012;38:2174–85.
42. Chen Y, Liang YB, Jiang P, Li F, Yu B, Yan F. Lipid/PLGA hybrid microbubbles as a versatile platform for noninvasive image-guided targeted drug delivery. ACS Appl Mater Interfaces 2019; 11:41842–52.

43. Peng YF, Li Q, Seekell RR, Kheir JN, Porter TM, Polizzotti BD. Tunable nonlinear acoustic reporters using micro- and nanosized air bubbles with porous polymeric hard shells. ACS Appl Mater Interfaces 2019;11:7–12.
44. Wang QZ, Xue CL, Zhao H, Qin Y, Zhang XH, Li Y. The fabrication of protein microbubbles with diverse gas core and the novel exploration on the role of interface introduction in protein crystallization. Colloids Surf A 2020;589:124471.
45. Streeter JE, Gessner R, Miles I, Dayton PA. Improving sensitivity in ultrasound molecular imaging by tailoring contrast agent size distribution: in vivo studies. Mol Imag 2010;9:87–95.
46. Lindner JR. Microbubbles in medical imaging: current applications and future directions. Nat Rev Drug Discov 2004;3: 527–32.
47. Frinking P, Segers T, Luan Y, Tranquart F. Three decades of ultrasound contrast agents: a review of the past, present and future improvements. Ultrasound Med Biol 2020;46:892–908.
48. Chomas JE, Dayton P, May D, Ferrara K. Threshold of fragmentation for ultrasonic contrast agents. J Biomed Opt 2001;6:141–50.
49. Greis C. Technical aspects of contrast-enhanced ultrasound (ceus) examinations: tips and tricks. Clin Hemorheol Microcirc 2014;58:89–95.
50. Ang TL, Kwek ABE, Wang LM. Diagnostic endoscopic ultrasound: technique, current status and future directions. Gut Liver 2018; 12:483–96.
51. Chong WK, Papadopoulou V, Dayton PA. Imaging with ultrasound contrast agents: current status and future. Abdom Radiol 2018;43:762–72.
52. Wang DY, Zhang XY, Sang YC, Qu Z, Su Q, Zhao J, et al. Influence of guided waves in bone on pulse-inversion contrast-enhanced ultrasound. Med Phys 2019;46:3475–82.
53. Muleki-Seya P, Xu K, Tanter M, Couture O. Ultrafast radial modulation imaging. IEEE Trans Ultrason Ferroelectr Freq Control 2020;67:598–611.
54. Viti J, Vos HJ, de Jong N, Guidi F, Tortoli P. Detection of contrast agents: plane wave versus focused transmission. IEEE Trans Ultrason Ferroelectr Freq Control 2016;63:203–11.
55. van Rooij T, Daeichin V, Skachkov I, de Jong N, Kooiman K. Targeted ultrasound contrast agents for ultrasound molecular imaging and therapy. Int J Hyperther 2015;31:90–106.
56. Kiessling F, Fokong S, Bzyl J, Lederle W, Palmowski M, Lammers T. Recent advances in molecular, multimodal and theranostic ultrasound imaging. Adv Drug Deliv Rev 2014;72:15–27.
57. Willmann JK, van Bruggen N, Dinkelborg LM, Gambhir SS. Molecular imaging in drug development. Nat Rev Drug Discov 2008;7:591–607.
58. Pochon S, Tardy I, Bussat P, Bettinger T, Brochot J, von Wronski M, et al. BR55: a lipopeptide-based VEGFR2-targeted ultrasound contrast agent for molecular imaging of angiogenesis. Invest Radiol 2010;45:89–95.
59. Zhang H, Tam S, Ingham ES, Mahakian LM, Lai CY, Tumbale SK, et al. Ultrasound molecular imaging of tumor angiogenesis with a neuropilin-1-targeted microbubble. Biomaterials 2015;56: 104–13.
60. Fisher NG, Christiansen JP, Klibanov A, Taylor RP, Kaul S, Lindner JR. Influence of microbubble surface charge on capillary transit and myocardial contrast enhancement. J Am Coll Cardiol 2002;40:811–9.
61. Khanicheh E, Mitterhuber M, Kinslechner K, Xu LF, Lindner JR, Kaufmann BA. Factors affecting the endothelial retention of targeted microbubbles: influence of microbubble shell design and cell surface projection of the endothelial target molecule. J Am Soc Echocardiogr 2012;25:460–6.
62. Lindner JR, Song J, Christiansen J, Klibanov AL, Xu F, Ley K. Ultrasound assessment of inflammation and renal tissue injury with microbubbles targeted to p-selectin. Circulation 2001;104:2107–12.
63. Ellegala DB, Leong-Poi H, Carpenter JE, Klibanov AL, Kaul S, Shaffrey ME, et al. Imaging tumor angiogenesis with contrast ultrasound and microbubbles targeted to alpha(v)beta3. Circulation 2003;108:336–41.
64. Yan F, Xu XX, Chen YH, Deng ZT, Liu HM, Xu JR, et al. A lipopeptide-based alpha v beta(3) integrin-targeted ultrasound contrast agent for molecular imaging of tumor angiogenesis. Ultrasound Med Biol 2015;41:2765–73.
65. Korpanty G, Carbon JG, Grayburn PA, Fleming JB, Brekken RA. Monitoring response to anticancer therapy by targeting microbubbles to tumor vasculature. Clin Cancer Res 2007;13: 323–30.
66. Alonso A, Della Martina A, Stroick M, Fatar M, Griebe M, Pochon S, et al. Molecular imaging of human thrombus with novel abciximab immunobubbles and ultrasound. Stroke 2007; 38:1508–14.
67. Wang XW, Hagemeyer CE, Hohmann JD, Leitner E, Armstrong PC, Jia F, et al. Novel single-chain antibody-targeted microbubbles for molecular ultrasound imaging of thrombosis validation of a unique noninvasive method for rapid and sensitive detection of thrombi and monitoring of success or failure of thrombolysis in mice. Circulation 2012;125:3117–26.
68. Armstrong PC, Peter K. GPIIb/IIIa inhibitors: from bench to bedside and back to bench again. Thromb Haemostasis 2012; 107:808–14.
69. Lindner JR. Molecular imaging of thrombus technology in evolution. Circulation 2012;125:3057–9.
70. Chadderdon SM, Belcik JT, Bader L, Kirigiti MA, Peters DM, Kievit P, et al. Proinflammatory endothelial activation detected by molecular imaging in obese nonhuman primates coincides with onset of insulin resistance and progressively increases with duration of insulin resistance. Circulation 2014;129:471–8.
71. Davidson BP, Kaufmann BA, Belcik JT, Xie A, Qi Y, Lindner JR. Detection of antecedent myocardial ischemia with multiselectin molecular imaging. J Am Coll Cardiol 2012;60:1690–7.
72. Wang HJ, Felt SA, Machtaler S, Guracar I, Luong R, Bettinger T, et al. Quantitative assessment of inflammation in a porcine acute terminal ileitis model: us with a molecularly targeted contrast agent. Radiology 2015;276:809–17.
73. Zhang X, Liu R, Dai Z. Multicolor nanobubbles for fret/ultrasound dual-modal contrast imaging. Nanoscale 2018;10:20347–53.
74. Xing ZW, Wang JR, Ke HT, Zhao B, Yue XL, Dai ZF, et al. The fabrication of novel nanobubble ultrasound contrast agent for potential tumor imaging. Nanotechnology 2010;21:145607.
75. Wu HP, Rognin NG, Krupka TM, Solorio L, Yoshiara H, Guenette G, et al. Acoustic characterization and pharmacokinetic analyses of new nanobubble ultrasound contrast agents. Ultrasound Med Biol 2013;39:2137–46.
76. Yin TH, Wang P, Zheng RQ, Zheng BW, Cheng D, Zhang XL, et al. Nanobubbles for enhanced ultrasound imaging of tumors. Int J Nanomed 2012;7:895–904.

77. Jugniot N, Massoud TF, Dahl JJ, Paulmurugan R. Biomimetic nanobubbles for triple-negative breast cancer targeted ultrasound molecular imaging. J Nanobiotechnol 2022;20: 1–14.
78. Mi X, Guo XM, Du HQ, Han M, Liu H, Luo YK, et al. Combined legumain- and integrin-targeted nanobubbles for molecular ultrasound imaging of breast cancer. Nanomed Nanotechnol Biol Med 2022;42:102533.
79. Johansen ML, Perera R, Abenojar E, Wang XN, Vincent J, Exner AA, et al. Ultrasound-based molecular imaging of tumors with ptpmu biomarker-targeted nanobubble contrast agents. Int J Mol Sci 2021;22:1983.
80. Su CH, Ren XJ, Nie F, Li TG, Lv WH, Li H, et al. Current advances in ultrasound-combined nanobubbles for cancer-targeted therapy: a review of the current status and future perspectives. RSC Adv 2021;11:12915–28.
81. Zlitni A, Gambhir SS. Molecular imaging agents for ultrasound. Curr Opin Chem Biol 2018;45:113–20.
82. Zhang WQ, Shi YH, Abd Shukor S, Vijayakumaran A, Vlatakis S, Wright M, et al. Phase-shift nanodroplets as an emerging sonoresponsive nanomaterial for imaging and drug delivery applications. Nanoscale 2022;14:2943–65.
83. Durham PG, Dayton PA. Applications of sub-micron low-boiling point phase change contrast agents for ultrasound imaging and therapy. Curr Opin Colloid Interface Sci 2021;56:101498.
84. Li KS, Liu YH, Zhang SM, Xu YF, Jiang JS, Yin FY, et al. Folate receptor-targeted ultrasonic PFOB nanoparticles: synthesis, characterization and application in tumor-targeted imaging. Int J Mol Med 2017;39:1505–15.
85. Liu JX, Shang TT, Wang FJ, Cao Y, Hao L, Ren JL, et al. Low-intensity focused ultrasound (LIFU)-induced acoustic droplet vaporization in phase-transition perfluoropentane nanodroplets modified by folate for ultrasound molecular imaging. Int J Nanomed 2017;12:911–23.
86. Rojas JD, Dayton PA. In vivo molecular imaging using low-boiling-point phase-change contrast agents: a proof of concept study. Ultrasound Med Biol 2019;45:177–91.
87. Huang YR, Vezeridis AM, Wang J, Wang Z, Thompson M, Mattrey RF, et al. Polymer-stabilized perfluorobutane nanodroplets for ultrasound imaging agents. J Am Chem Soc 2017;139:15–8.
88. Paproski RJ, Forbrich A, Huynh E, Chen J, Lewis JD, Zheng G, et al. Porphyrin nanodroplets: sub-micrometer ultrasound and photoacoustic contrast imaging agents. Small 2016;12:371–80.
89. Wu MX, Xiong HB, Zou HM, Li M, Li P, Zhou Y, et al. A laser-activated multifunctional targeted nanoagent for imaging and gene therapy in a mouse xenograft model with retinoblastoma y79 cells. Acta Biomater 2018;70:211–26.
90. Spatarelu CP, Van Namen A, Luke GP. Optically activatable double-drug-loaded perfluorocarbon nanodroplets for on-demand image-guided drug delivery. ACS Appl Nano Mater 2021;4:8026–38.
91. Sheng DL, Deng LM, Li P, Wang ZG, Zhang QX. Perfluorocarbon nanodroplets with deep tumor penetration and controlled drug delivery for ultrasound/fluorescence imaging guided breast cancer therapy. ACS Biomater Sci Eng 2021;7:605–16.
92. Zhang K, Li P, Chen HR, Bo XW, Li XL, Xu HX. Continuous cavitation designed for enhancing radiofrequency ablation via a special radiofrequency solidoid vaporization process. ACS Nano 2016;10:2549–58.
93. Xu JS, Chen Y, Deng LM, Liu JX, Cao Y, Li P, et al. Microwave-activated nanodroplet vaporization for highly efficient tumor ablation with real-time monitoring performance. Biomaterials 2016;106:264–75.
94. Carlier B, Heymans SV, Nooijens S, Toumia Y, Ingram M, Paradossi G, et al. Proton range verification with ultrasound imaging using injectable radiation sensitive nanodroplets: a feasibility study. Phys Med Biol 2020;65:065013.
95. Min HS, Son S, You DG, Lee TW, Lee J, Lee S, et al. Chemical gas-generating nanoparticles for tumor-targeted ultrasound imaging and ultrasound-triggered drug delivery. Biomaterials 2016;108:57–70.
96. Cho S, Hwang O, Lee I, Lee G, Yoo D, Khang G, et al. Chemiluminescent and antioxidant micelles as theranostic agents for hydrogen peroxide associated-inflammatory diseases. Adv Funct Mater 2012;22:4038–43.
97. Kang C, Cho W, Park M, Kim J, Park S, Shin D, et al. H_2O_2-triggered bubble generating antioxidant polymeric nanoparticles as ischemia/reperfusion targeted nanotheranostics. Biomaterials 2016;85:195–203.
98. Heo J, Lim CK, Min HS, Lee KE, Jeong K, Seo YH, et al. Rational design of inflammation-responsive inflatable nanogels for ultrasound molecular imaging. Chem Mater 2019;31:2905–12.
99. Liu T, Zhang N, Wang Z, Wu M, Chen Y, Ma M, et al. Endogenous catalytic generation of O_2 bubbles for in situ ultrasound-guided high intensity focused ultrasound ablation. ACS Nano 2017;11: 9093–102.
100. Alphandery E. Nanomaterials as ultrasound theragnostic tools for heart disease treatment/diagnosis. Int J Mol Sci 2022;23: 1683.
101. Chen F, Ma M, Wang JX, Wang F, Chern SX, Zhao ER, et al. Exosome-like silica nanoparticles: a novel ultrasound contrast agent for stem cell imaging. Nanoscale 2017;9:402–11.
102. Wu HX, Shi HL, Zhang H, Wang X, Yang Y, Yu C, et al. Prostate stem cell antigen antibody-conjugated multiwalled carbon nanotubes for targeted ultrasound imaging and drug delivery. Biomaterials 2014;35:5369–80.
103. Casciaro S, Conversano F, Ragusa A, Malvindi MA, Franchini R, Greco A, et al. Optimal enhancement configuration of silica nanoparticles for ultrasound imaging and automatic detection at conventional diagnostic frequencies. Invest Radiol 2010;45: 715–24.
104. Li XY, Xia SJ, Ji R, Zhan WW, Zhou W. Evaluation of microwave ablation in 4T1 breast tumor by a novel VEFGR2 targeted ultrasound contrast agents. Front Oncol 2021;11:690152.
105. Li XY, Xia SJ, Zhou W, Ji R, Zhan WW. Targeted Fe-doped silica nanoparticles as a novel ultrasound-magnetic resonance dual-mode imaging contrast agent for HER2-positive breast cancer. Int J Nanomed 2019;14:2397–413.
106. Liberman A, Wang J, Lu N, Viveros RD, Allen CA, Mattrey RF, et al. Mechanically tunable hollow silica ultrathin nanoshells for ultrasound contrast agents. Adv Funct Mater 2015;25:4049–57.
107. Yildirim A, Chattaraj R, Blum NT, Goldscheitter GM, Goodwin AP. Stable encapsulation of air in mesoporous silica nanoparticles: fluorocarbon-free nanoscale ultrasound contrast agents. Adv Healthcare Mater 2016;5:1290–8.
108. Gu FF, Hu CL, Xia QM, Gong CA, Gao S, Chen ZJ. Aptamer-conjugated multi-walled carbon nanotubes as a new targeted ultrasound contrast agent for the diagnosis of prostate cancer. J Nanopart Res 2018;20:303.

109. Li W, Hou WQ, Guo XM, Luo LH, Li QP, Zhu CQ, et al. Temperature-controlled, phase-transition ultrasound imaging-guided photothermal-chemotherapy triggered by NIR light. Theranostics 2018;8:3059–73.
110. Guan QQ, Wang CN, Wu D, Wang W, Zhang CY, Liu J, et al. Cerasome-based gold-nanoshell encapsulating l-menthol for ultrasound contrast imaging and photothermal therapy of cancer. Nanotechnology 2019;30:015101.
111. Zhao YJ, Song WX, Wang D, Ran HT, Wang RH, Yao YZ, et al. Phase-shifted PFH@PLGA/Fe_3O_4 nanocapsules for MRI/US imaging and photothermal therapy with near-infrared irradiation. ACS Appl Mater Interfaces 2015;7:14231–42.
112. Teng ZG, Wang RH, Zhou Y, Kolios M, Wang YJ, Zhang N, et al. A magnetic droplet vaporization approach using perfluorohexane-encapsulated magnetic mesoporous particles for ultrasound imaging and tumor ablation. Biomaterials 2017; 134:43–50.
113. Jia XQ, Cai XJ, Chen Y, Wang SG, Xu HX, Zhang K, et al. Perfluoropentane-encapsulated hollow mesoporous prussian blue nanocubes for activated ultrasound imaging and photothermal therapy of cancer. ACS Appl Mater Interfaces 2015;7:4579–88.
114. Zhang N, Cai XJ, Gao W, Wang RH, Xu CY, Yao YZ, et al. A multifunctional theranostic nanoagent for dual-mode image-guided HIFU/chemo-synergistic cancer therapy. Theranostics 2016;6:404–17.
115. Gao S, Wang GH, Qin ZN, Wang XY, Zhao GQ, Ma QJ, et al. Oxygen-generating hybrid nanoparticles to enhance fluorescent/photoacoustic/ultrasound imaging guided tumor photodynamic therapy. Biomaterials 2017;112:324–35.
116. Yang F, Hu SL, Zhang Y, Cai XW, Huang Y, Wang F, et al. A hydrogen peroxide-responsive O_2 nanogenerator for ultrasound and magnetic-resonance dual modality imaging. Adv Mater 2012;24:5205–11.
117. Feng QH, Zhang WX, Yang XM, Li YZ, Hao YW, Zhang HL, et al. Ph/ultrasound dual-responsive gas generator for ultrasound imaging-guided therapeutic inertial cavitation and sonodynamic therapy. Adv Healthcare Mater 2018;7:1700957.
118. Chen SS, Xu XL, Zhou BY, Tian J, Luo BM, Zhang LM. Acidic ph-activated gas-generating nanoparticles with pullulan decorating for hepatoma-targeted ultrasound imaging. ACS Appl Mater Interfaces 2019;11:22194–205.
119. Vidallon MLP, Douek AM, Quek A, McLiesh H, Kaslin J, Tabor RF, et al. Gas-generating, ph-responsive calcium carbonate hybrid particles with biomimetic coating for contrast-enhanced ultrasound imaging. Part Part Syst Char 2020;37:1900471.
120. Maresca D, Lakshmanan A, Abedi M, Bar-Zion A, Farhadi A, Lu GJ, et al. Biomolecular ultrasound and sonogenetics. Annu Rev Chem Biomol Eng 2018;9:229–52.
121. Lu GJ, Farhadi A, Mukherjee A, Shapiro MG. Proteins, air and water: reporter genes for ultrasound and magnetic resonance imaging. Curr Opin Chem Biol 2018;45:57–63.
122. Ezzeldin HM, Klauda JB, Solares SD. Modeling of the major gas vesicle protein, GvpA: from protein sequence to vesicle wall structure. J Struct Biol 2012;179:18–28.
123. Piraner DI, Farhadi A, Davis HC, Wu D, Maresca D, JO S, et al. Going deeper: biomolecular tools for acoustic and magnetic imaging and control of cellular function. Biochemistry 2017;56: 5202–9.
124. Lu GJ, Farhadi A, JO S, Lee-Gosselin A, Barnes SR, Lakshmanan A, et al. Acoustically modulated magnetic resonance imaging of gas-filled protein nanostructures. Nat Mater 2018;17:456–63.
125. Cherin E, Melis JM, Bourdeau RW, Yin M, Kochmann DM, Foster FS, et al. Acoustic behavior of *Halobacterium salinarum* gas vesicles in the high-frequency range: experiments and modeling. Ultrasound Med Biol 2017;43:1016–30.
126. Maresca D, Lakshmanan A, Lee-Gosselin A, Melis JM, Ni YL, Bourdeau RW, et al. Nonlinear ultrasound imaging of nanoscale acoustic biomolecules. Appl Phys Lett 2017;110:073704.
127. Maresca D, Sawyer DP, Renaud G, Lee-Gosselin A, Shapiro MG. Nonlinear x-wave ultrasound imaging of acoustic biomolecules. Phys Rev X 2018;8:041002.
128. Yan J, Yin M, Foster FS, Demore CEM. Tumor contrast imaging with gas vesicles by circumventing the reticuloendothelial system. Ultrasound Med Biol 2020;46:359–68.
129. Wang GH, Song L, Hou XD, Kala S, Wong KF, Tang LY, et al. Surface-modified GVs as nanosized contrast agents for molecular ultrasound imaging of tumor. Biomaterials 2020;236: 119803.
130. Mace E, Montaldo G, Cohen I, Baulac M, Fink M, Tanter M. Functional ultrasound imaging of the brain. Nat Methods 2011;8: 662–4.
131. Deffieux T, Demene C, Pernot M, Tanter M. Functional ultrasound neuroimaging: a review of the preclinical and clinical state of the art. Curr Opin Neurobiol 2018;50:128–35.
132. Mace E, Montaldo G, Trenholm S, Cowan C, Brignall A, Urban A, et al. Whole- brain functional ultrasound imaging reveals brain modules for visuomotor integration. Neuron 2018;100:1241–51.
133. Errico C, Osmanski BF, Pezet S, Couture O, Lenkei Z, Tanter M. Transcranial functional ultrasound imaging of the brain using microbubble-enhanced ultrasensitive Doppler. Neuroimage 2016;124:752–61.
134. Maresca D, Payen T, Lee-Gosselin A, Ling B, Malounda D, Demene C, et al. Acoustic biomolecules enhance hemodynamic functional ultrasound imaging of neural activity. Neuroimage 2020;209:116467.
135. Lakshmanan A, Jin ZY, Nety SP, Sawyer DP, Lee-Gosselin A, Malounda D, et al. Acoustic biosensors for ultrasound imaging of enzyme activity. Nat Chem Biol 2020;16:988–96.
136. Farhadi A, Ho G, Kunth M, Ling B, Lakshmanan A, Lu GJ, et al. Recombinantly expressed gas vesicles as nanoscale contrast agents for ultrasound and hyperpolarized MRI. AIChE J 2018;64: 2927–33.
137. Shieh YW, Minguez P, Bork P, Auburger JJ, Guilbride DL, Kramer G, et al. Operon structure and cotranslational subunit association direct protein assembly in bacteria. Science 2015; 350:678–80.
138. Natan E, Wells JN, Teichmann SA, Marsh JA. Regulation, evolution and consequences of cotranslational protein complex assembly. Curr Opin Struct Biol 2017;42:90–7.
139. Sawyer DP, Bar-Zion A, Farhadi A, Shivaei S, Ling B, Lee-Gosselin A, et al. Ultrasensitive ultrasound imaging of gene expression with signal unmixing. Nat Methods 2021;18:945–52.

Supplementary Material: The online version of this article offers supplementary material (https://doi.org/10.1515/mr-2022-0020).